Supporting Information

From Zero-dimensional to One-dimensional Chain N-oxide Bridged Compounds with Enhanced Single-Molecule Magnetic Performance

Ling Zhang,[a] Peng Chen,[a] Hong-Feng Li,[a] Yong-Mei Tian,[*a] Peng-Fei Yan [a] and Wen-Bin Sun[*a]

a. Key Laboratory of Functional Inorganic Material Chemistry Ministry of Education, School of Chemistry and Material Science Heilongjiang University, 74 Xuefu Road, Harbin 150080, P. R. China.

E-mail: wenbinsun@126.com

Table S1. Crystallographic parameters of all complexes.

	1Dy	***1Y***	***1Gd***	***2Dy***
formula	$C_{70}H_{46}Dy_2F_{18}N_2O_{14}$	$C_{76}H_{60}F_{18}N_2O_{14}Y_2$	$C_{76}H_{60}F_{18}Gd_2N_2O_{14}$	$C_{71}H_{47}Dy_2F_{18}N_2O_{14.5}$
FW ($g.mol^{-1}$)	1806.09	1745.08	1881.76	1827.10
Crystal system	Monoclinic	Monoclinic	Monoclinic	monoclinic
Space group	*$P2_1/n$*	*C2/c*	*C2/c*	*$P2_1/c$*
Temperature (K)	293.15	296.15	296.15	293
a (Å)	14.9410(6)	30.584(4)	30.888(3)	24.291(2)
b (Å)	14.3461(12)	11.6402(14)	11.6448(10)	14.5614(16)
c (Å)	17.1220(8)	23.067(3)	23.2385(19)	23.223(2)
α (°)	90	90	90	90
β (°)	101.175(4)	108.878(2)	109.5270(10)	117.676(12)
γ (°)	90	90	90	90
V ($Å^3$)	3600.4(4)	7770.3(16)	7877.9(11)	7274.4(14)
ρ_{cacd} ($g.cm^{-3}$)	1.666	1.492	1.587	1.668
μ (mm^{-1})	2.169	1.592	1.774	2.149
F (000)	1772.0	3528.0	3728.0	3588.0
Collected reflections	33723	25297	34589	22451
Independent reflections	9389	6860	9764	13211
R_{int}	0.0277	0.0340	0.0215	0.0606
R_1 [$I > 2\sigma(I)$]	0.0425	0.0409	0.0334	0.1047
wR_2 (all data)	0.0892	0.1029	0.1163	0.2867
GOF	1.118	1.041	0.739	1.055

Table S2. Selected bond lengths (Å) and angles (°) for **1Dy**

Dy1-O1	2.350(3)	Dy1-O4	2.337(3)
Dy1-O2	2.310(3)	Dy1-O3	2.307(3)
Dy1-O6	2.343(3)	Dy1-O5	2.317(3)
Dy1-O7	2.388(3)	Dy1-O7′	2.415(2)
O(1)-Dy(1)-O(2)	71.82(10)	O(1)-Dy(1)-O(6)	144.14(11)
O(1)-Dy(1)-O(7′)	124.87(10)	O(1)-Dy(1)-O(7)	78.33(9)
O(4)-Dy(1)-O(1)	132.94(11)	O(4)-Dy(1)-O(2)	77.80(13)
O(4)-Dy(1)-O(6)	74.87(13)	O(4)-Dy(1)-O(7′)	78.60(9)

O(4)-Dy(1)-O(7)	141.04(9)	O(2)-Dy(1)-O(6)	143.82(11)
O(2)-Dy(1)-O(7)	96.30(11)	O(2)-Dy(1)-O(7′)	75.19(10)
O(3)-Dy(1)-O(1)	73.84(11)	O(3)-Dy(1)-O(4)	75.84(12)
O(3)-Dy(1)-O(2)	91.44(13)	O(3)-Dy(1)-O(6)	101.97(13)
O(3)-Dy(1)-O(5)	75.84(12)	O(3)-Dy(1)-O(7)	147.09(9)
O(3)-Dy(1)-O(7′)	149.61(10)	O(6)-Dy(1)-O(7)	90.38(11)
O(6)-Dy(1)-O(7′)	90.38(11)	O(5)-Dy(1)-O(1)	73.55(10)
O(5)-Dy(1)-O(4)	126.00(12)	O(5)-Dy(1)-O(2)	145.21(10)
O(5)-Dy(1)-O(6)	70.96(11)	O(5)-Dy(1)-O(7)	79.75(10)
O(5)-Dy(1)-O(7′)	129.58(10)	O(7′)-Dy(1)-O(7)	62.80(10)

Table S3. Selected bond lengths (Å) and angles (°) for **2Dy**

Dy1-O4	2.305(9)	Dy2-O14′	2.427(9)
Dy1-O7′	2.394(9)	Dy2-O14	2.390(9)
Dy1-O7	2.425(9)	Dy2-O12	2.356(10)
Dy1-O5	2.334(10)	Dy2-O11	2.319(11)
Dy1-O3	2.301(12)	Dy2-O13	2.366(11)
Dy1-O1	2.317(11)	Dy2-O9	2.315(10)
Dy1-O2	2.311(10)	Dy2-O10	2.289(13)
Dy1-O6	2.360(12)	Dy2-O8	2.341(13)
Dy1′-O7-Dy1	116.5(3)	Dy2-O14-Dy2 ′	117.0(3)
O4-Dy1-O7	75.0(3)	O14′-Dy2-O14	63.0(3)
O4-Dy1-O7′	117.1(3)	O12-Dy2-O14′	79.3(3)
O4-Dy1-O5	76.4(4)	O12-Dy2-O14	127.3(3)
O4-Dy1-O1	140.2(4)	O12-Dy2-O13	70.6(3)
O4-Dy1-O2	74.1(3)	O11-Dy2-O14′	141.5(3)
O4-Dy1-O6	143.4(4)	O11-Dy2-O14	78.5(3)
O7′-Dy1-O7	63.5(3)	O11-Dy2- O12	128.0(4)
O5-Dy1-O7′	82.2(3)	O11-Dy2- O13	77.3(4)
O5-Dy1-O6	135.5(3)	O11-Dy2- O8	75.6(4)
O3-Dy1-O4	72.4(4)	O13-Dy2- O14	74.4(4)
O3-Dy1-O7	72.4(4)	O13-Dy2- O14′	90.8(4)
O3-Dy1-O7′	74.6(4)	O9-Dy2- O14′	76.7(4)
O3-Dy1-O5	145.2(4)	O9-Dy2- O14	124.1(4)
O3-Dy1-O1	79.1(4)	O9-Dy2- O12	75.9(4)
O3-Dy1-O2	78.7(4)	O9-Dy2-O11	131.0(4)
O3-Dy1-O6	141.7(4)	O9-Dy2-O13	145.9(4)
O1-Dy1-O7	140.6(3)	O9-Dy2- O8	70.5(4)
O1-Dy1- O7′	80.6(3)	O10-Dy2- O14′	146.5(3)
O1-Dy1- O5	117.2(4)	O10-Dy2- O14	150.4(3)
O1-Dy1- O6	117.2(4)	O10-Dy2- O12	74.9(4)
O2-Dy1- O7′	145.6(3)	O10-Dy2- O11	72.0(4)
O2-Dy1- O7	146.2(3)	O10-Dy2- O13	100.3(5)
O2-Dy1- O5	77.6(4)	O10-Dy2-O8	94.6(5)
O2-Dy1-O1	73.2(3)	O8-Dy2-O14′	76.0(4)
O2-Dy1-O6	73.2(3)	O8-Dy2-O14	95.1(4)
O6-Dy1-O7′	75.4(4)	O8-Dy2-O12	146.4(4)
O6-Dy1-O7	82.3(4)	O8-Dy2-O13	143.0(4)

Table S4. Continuous Shape Measures (CShMs) of the coordination geometry for Dy(III) ion in complexes **1Dy** and **2Dy** (S values calculated with the Shape program). The *S* values indicated the proximity to the ideal polyhedron, thus, a $S = 0$ corresponds to the non-distorted polyhedron. The three closer ideal geometry to the real complexes are listed and below is the symmetry and description for each polyhedron.

	1Dy (Dy$_1$)	**2Dy (Dy$_1$)**	**2Dy (Dy$_2$)**
TDD-8	0.431	1.962	0.304
SAPR-8	2.027	0.539	2.404
BTPR-8	2.108	1.671	2.406

TDD-8	D2d	Triangular dodecahedron
SAPR-8	D4d	Square antiprism
BTPR-8	C2v	Biaugmented trigonal prism

Table S5. Energy barriers obtained from the Arrhenius law fitting and Equation 2 of the out-of-phase (χ'') ac susceptibility data under zero dc field.

Relaxation processes	Orbach processes		Raman and Orbach processes			
	U_{eff}/κ_B (K)	τ_0 (s)	C ($s^{-1}\cdot K^{-n}$)	n	U_{eff}/κ_B (K)	τ_0 (s)
1Dy	72.04	1.78×10^{-6}	3.65×10^{-3}	5.08	88.51	2.32×10^{-6}
2Dy	86.98	1.02×10^{-6}	4.80×10^{-3}	4.72	108.98	5.49×10^{-7}
1a	50.13	1.42×10^{-5}	3.01×10^{-2}	3.88	61.17	1.12×10^{-5}
2a	50.66	9.26×10^{-6}	5.56	1.22	46.14	1.51×10^{-5}

Table S6. Energy barriers obtained from the Arrhenius law fitting and Equation 1 of the out-of-phase (χ'') ac susceptibility data under applied dc field.

Relaxation process	Orbach processes		Raman and Orbach processes			
	U_{eff}/κ_B (K)	τ_0 (s)	C ($s^{-1}\cdot K^{-n}$)	n	U_{eff}/κ_B (K)	τ_0 (s)
1Dy	71.04	1.63×10^{-6}	7.75×10^{-3}	4.82	85.35	1.77×10^{-6}
2Dy	83.25	1.12×10^{-6}	1.64×10^{-2}	4.17	97.89	7.32×10^{-7}
1a	59.04	9.35×10^{-6}	3.96×10^{-2}	3.07	63.54	7.42×10^{-6}
2a	59.32	5.84×10^{-6}	1.05×10^{-2}	4.24	58.64	8.98×10^{-6}

Table S7. Best fitted parameters (χ_T, χ_S, τ and α) with the extended Debye model for complex **1Dy** at 0 Oe in the temperature range 5-16K.

T/ K	χ_S / cm^3 mol^{-1}	χ_T / cm^3 mol^{-1}	τ/s	α	R

5	0.03799	3.97469	0.07774	0.03399	3.30E-005
6	0.03990	3.39124	0.03057	0.02648	2.75E-005
7	0.03983	2.96212	0.01377	0.01832	2.10E-005
8	0.04186	2.62889	0.00677	0.00850	2.90E-005
9	0.04100	2.37161	0.00360	0.01085	2.21E-005
10	0.04089	2.15932	0.00203	0.00914	2.46E-005
11	0.05360	1.97515	0.00120	0.00156	2.94E-005
12	0.06098	1.82716	0.00074	0.00005	2.67E-005
13	0.07467	1.70061	0.00048	0.00184	3.45E-005
14	0.08590	1.58982	0.00032	0.00114	3.88E-005
15	0.13334	1.49357	0.00021	0.00154	4.60E-005
16	0.18104	1.40459	0.00015	0.00425	4.38E-005

Table S8. Best fitted parameters (χ_T, χ_S, τ and α) with the extended Debye model for complex **2Dy** at 0 Oe in the temperature range 5-18K.

T/ K	χ_S / cm^3 mol^{-1}	χ_T / cm^3 mol^{-1}	τ/s	α	R
5	0.06812	3.22264	0.09998	0.14598	9.50E-004
6	0.04537	3.05754	0.05008	0.17733	6.01E-004
7	0.03078	2.75650	0.02427	0.18701	4.77E-004
8	0.02270	2.48125	0.01257	0.18708	3.62E-004
9	0.02394	2.23671	0.00674	0.18624	2.66E-004
10	0.02247	2.04896	0.00388	0.18935	2.22E-004
11	0.02948	1.88215	0.00229	0.19435	2.31E-004
12	0.03108	1.73775	0.00139	0.20390	2.42E-004
13	0.06579	1.61384	0.00089	0.20269	2.43E-004
14	0.17210	1.50567	0.00062	0.19182	2.57E-004
15	0.21593	1.41041	0.00040	0.20343	1.62E-004
16	0.35709	1.32451	0.00031	0.17034	8.54E-005
17	0.56290	1.24814	0.00027	0.07884	3.55E-005
18	0.53956	1.18609	0.00016	0.11352	7.19E-005

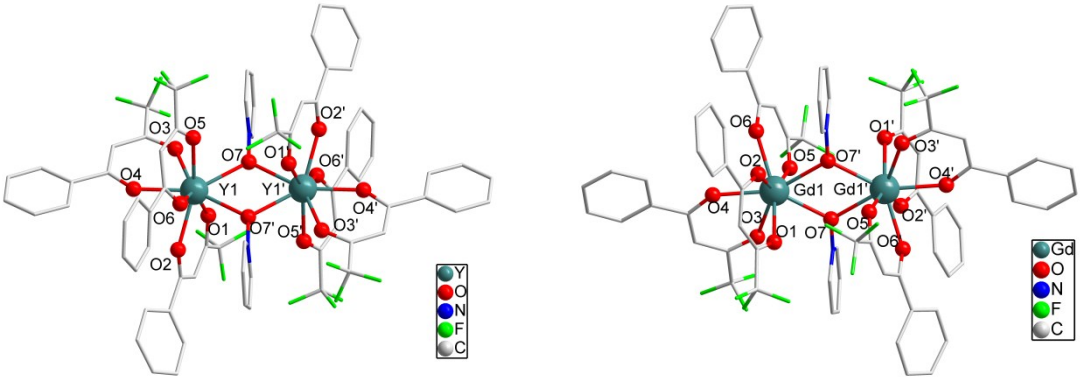

Fig. S1. Molecular structure of complexes **1Y** (left) and **1Gd** (right). Colour code: Y and Gd (teal), O (red), N (blue), F (green), C (grey). H atoms and disorder atoms were omitted for clarity.

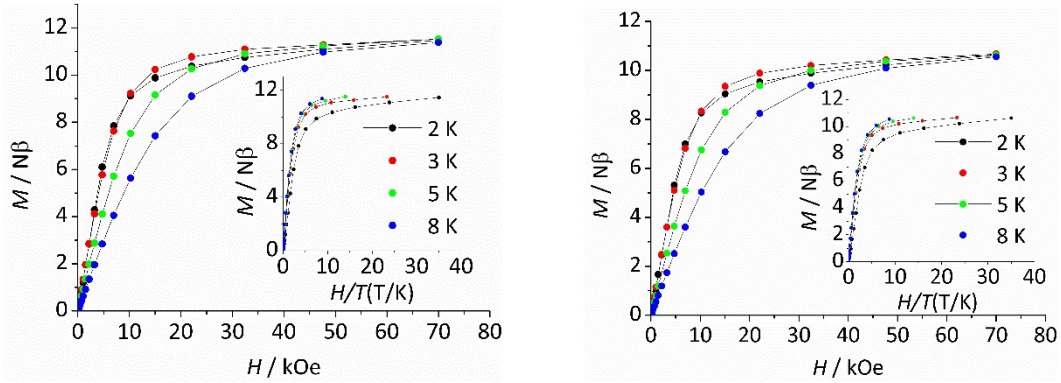

Figure S2. Field dependences of magnetization in the field range 0−70 kOe and temperature range 2−8 K for complex **1Dy** (left) and **2Dy** (right).Inset: *M* vs. *H/T* plots at different temperatures 2, 3, 5 and 8 K.

The $\chi_m T$ values of the **1Gd** and **2Gd** are 14.91 and 14.78 cm^3 K mol^{-1}at 300 K, respectively, somewhat smaller than the expected value 15.76 cm^3 K mol^{-1} of two uncoupled $^8S_{7/2}$ centers. With the known isotropic interaction, the Hamiltonian $H = -JS_{Gd1} \cdot S_{Gd2}$ results in the formula for the temperature dependence of the molar magnetic susceptibility in equation (S1), where *g* is the Landé factor, *β* is the Bohr magneton, *N* is the Avogadro number, and *k* is the Boltzmann constant and $x = -J/kT$.

$$\chi_m T = \frac{2Ng^2\mu_B^2\left(e^x + 5e^{3x} + 14e^{6x} + 30e^{10x} + 55e^{15x} + 91e^{21}\right.}{k \quad 1 + 3e^x + 5e^{3x} + 7e^{6x} + 9e^{10x} + 11e^{15x} + 13e} \quad \text{(S1)}$$

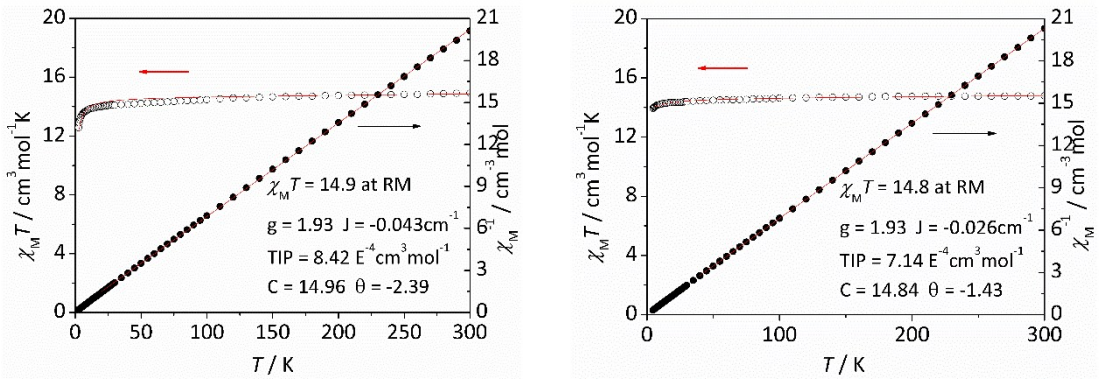

Fig. S3. Temperature dependence of the $\chi_M T$ values T measured at 1000 Oe for **1Gd** (left) and **2Gd** (right). The solid line corresponds to the best fit for **1Gd** and **2Gd**.

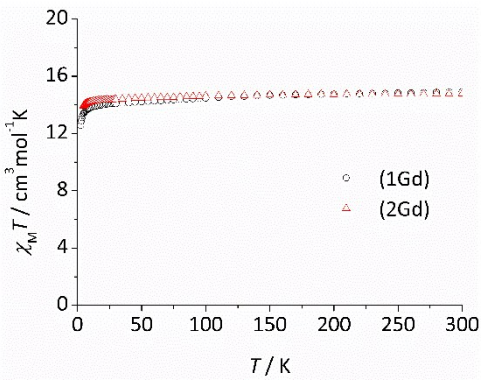

Fig. S4. Temperature dependence of the $\chi_M T$ values T measured at 1000 Oe for **1Gd** and **2Gd**.

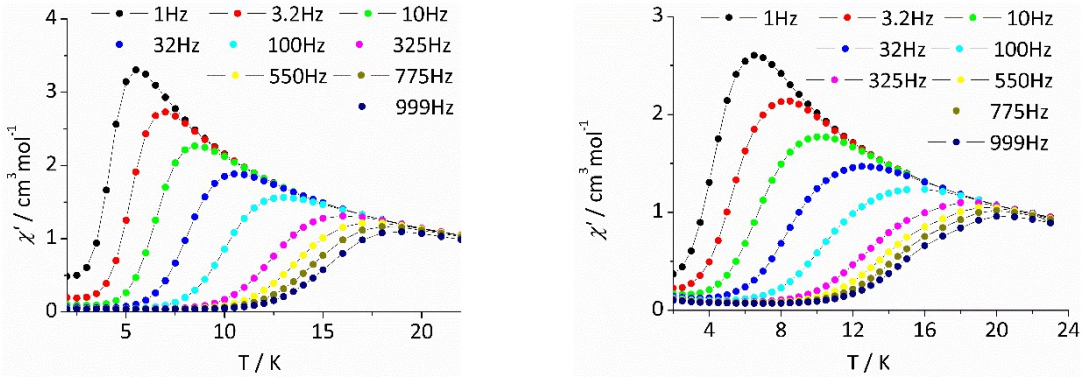

Fig. S5. Temperature dependence of the in-phase (χ') for complexes **1Dy** (left) and **2Dy** (right) without dc field.

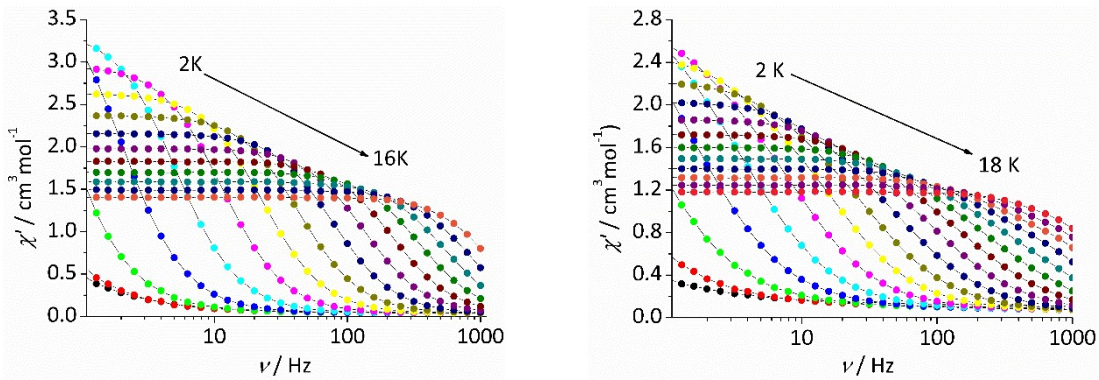

Fig. S6. Frequency dependence of the in-phase (χ') for complexes **1Dy** (left) and **2Dy** (right) without dc field.

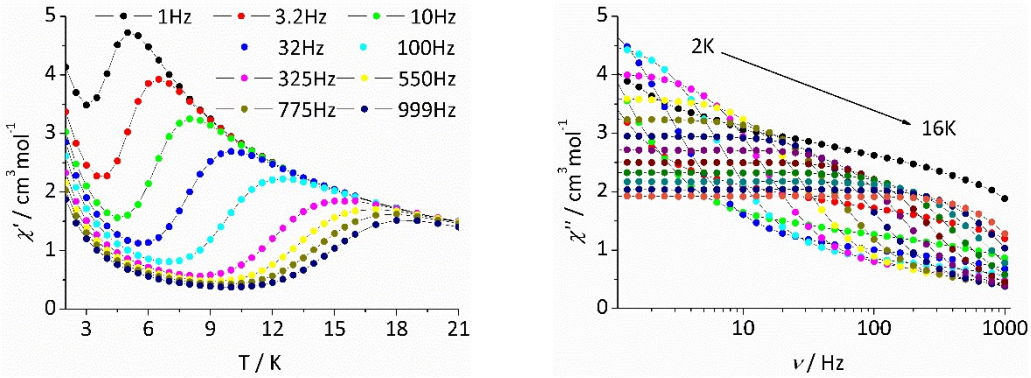

Fig. S7. The temperature (left) and frequency (right) dependence of out-of-phase (χ′) ac susceptibility for **1Dy** under 1500 Oe dc field.

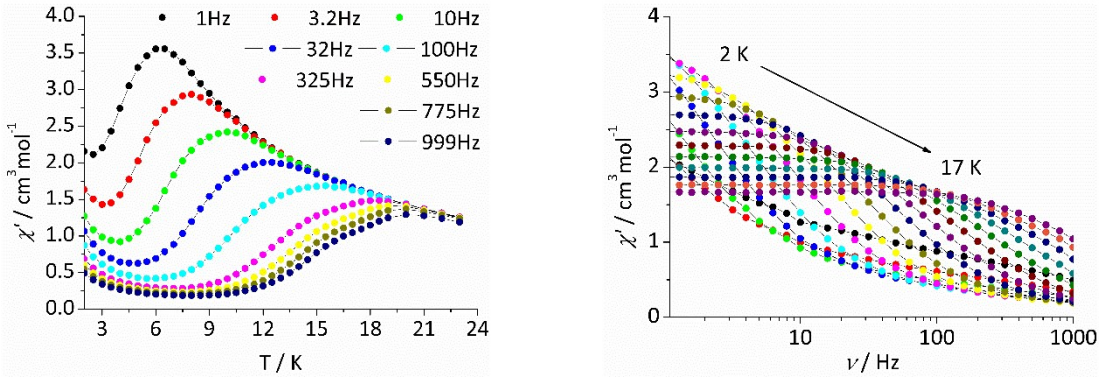

Fig. S8. The temperature (left) and frequency (right) dependence of out-of-phase (χ′) ac susceptibility for **2Dy** under 1900 Oe dc field.

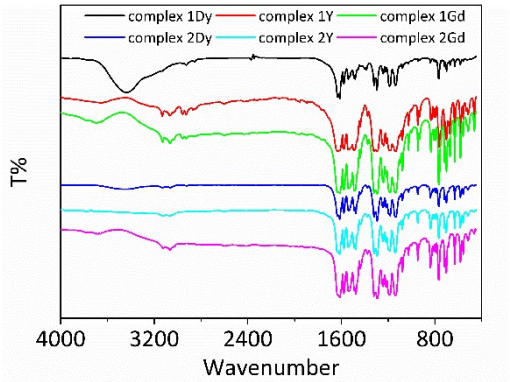

Fig. S9. FT-IR spectra of all th e complexes.

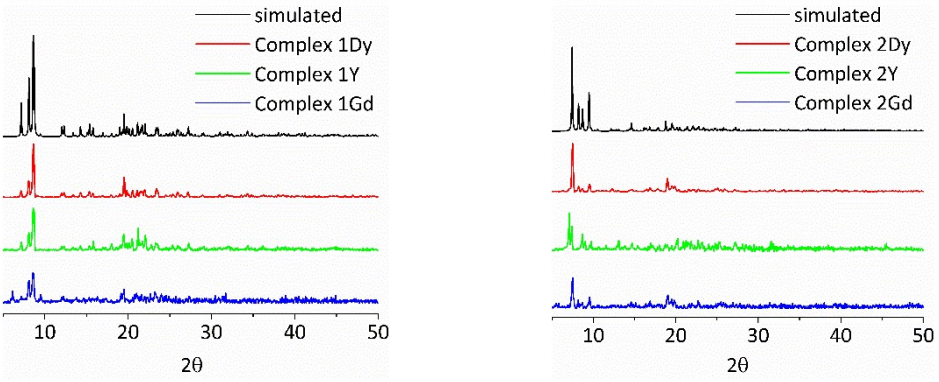

Fig. S10. PXRD analysis of all the complexes.

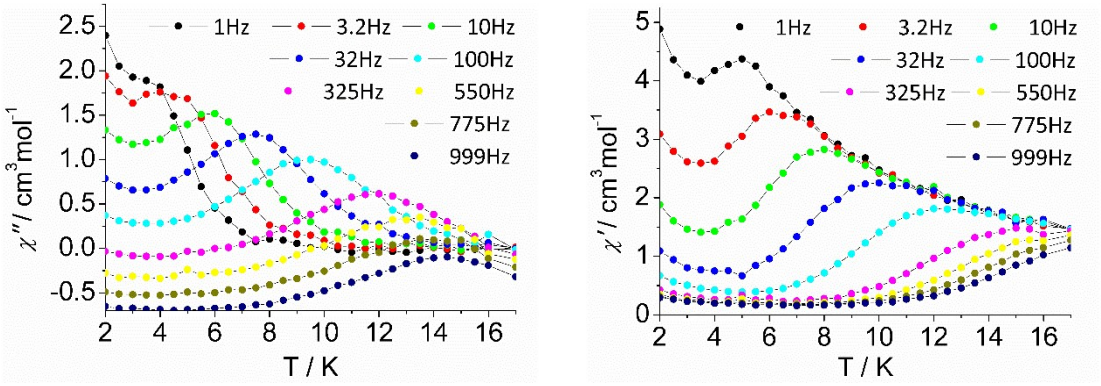

Fig. S11. Temperature dependence of the out-of-phase (χ'') and in-phase (χ') for **1a** without dc field.

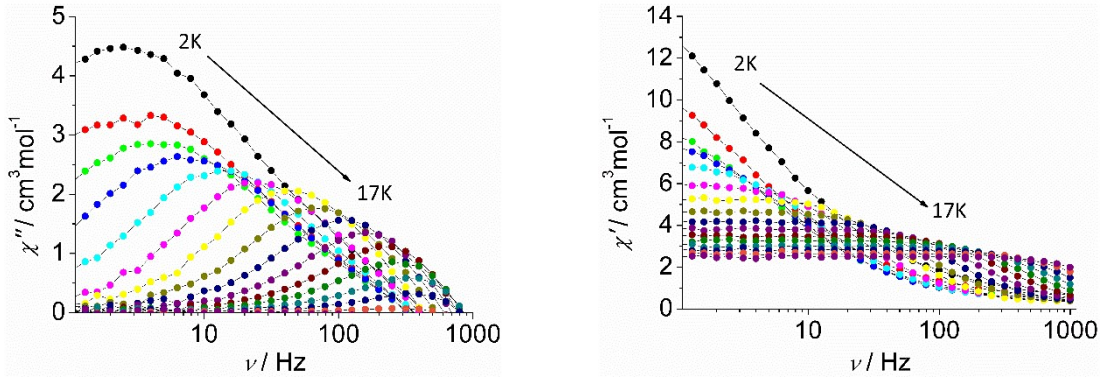

Fig. S12. Frequency dependence of the out-of-phase (χ'') and in-phase (χ') for **1a** without dc fiel.

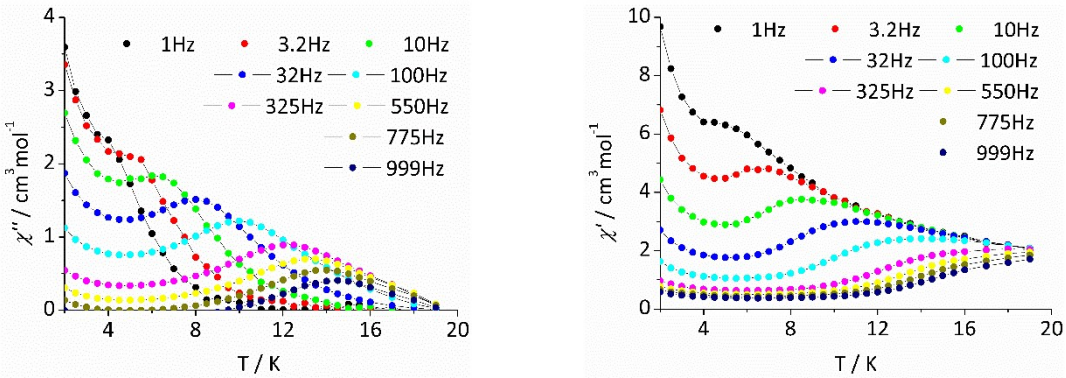

Fig. S13. Temperature dependence of the out-of-phase (χ'') and in-phase (χ') for **2a** without dc field.

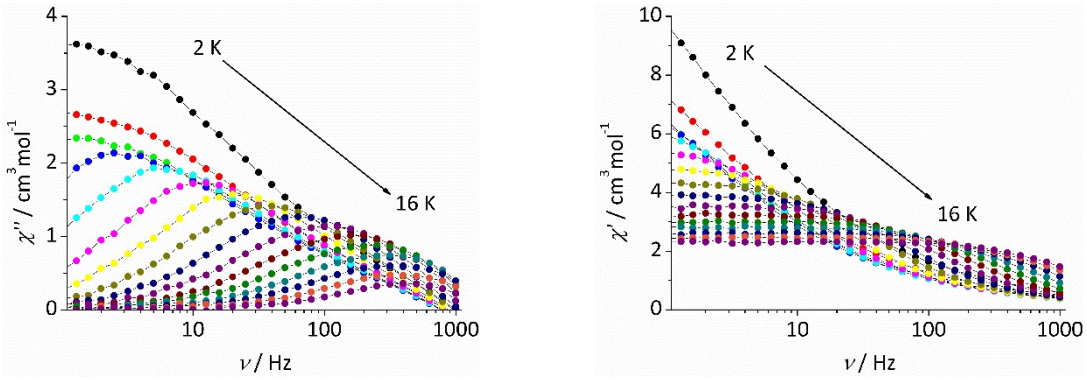

Fig. S14. Frequency dependence of the out-of-phase (χ'') and in-phase (χ') for **2a** without dc fiel.

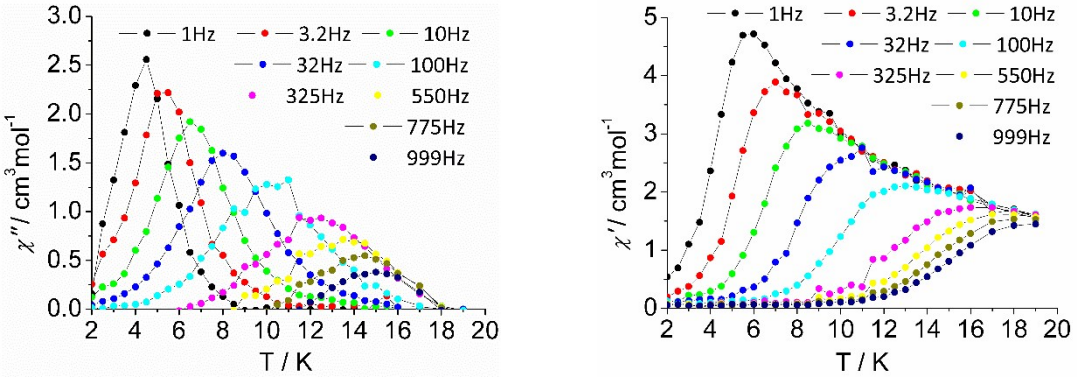

Fig. S15. Temperature dependence of the out-of-phase (χ'') and in-phase (χ') for **1a** under 1500 Oe dc field.

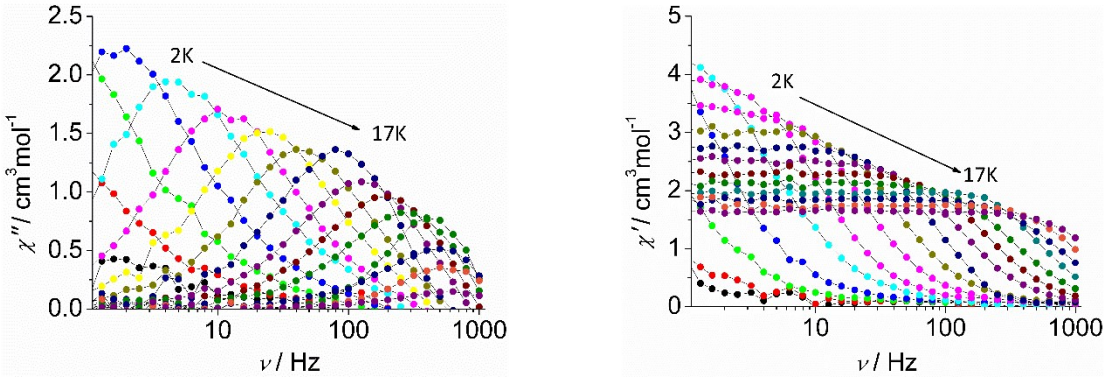

Fig. S16. Frequency dependence of the out-of-phase (χ'') and in-phase (χ') for **1a** under 1500 Oe dc field.

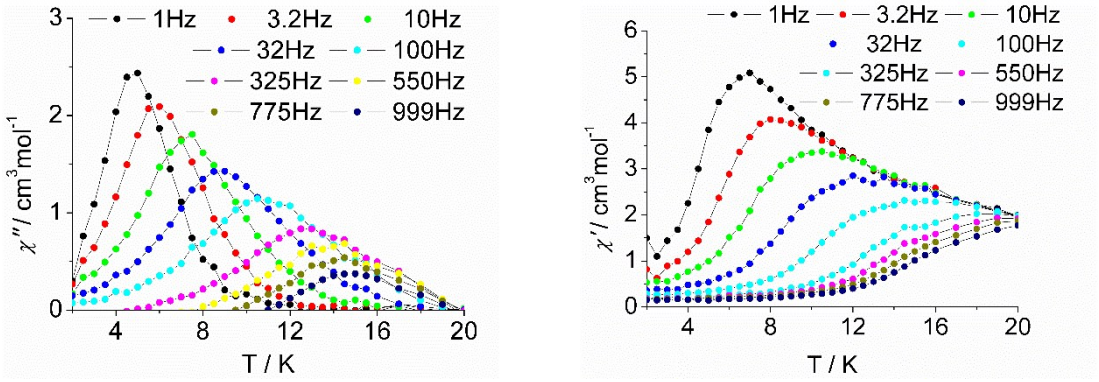

Fig. S17. Temperature dependence of the out-of-phase (χ'') and in-phase (χ') for **2a** under 1500 Oe dc field.

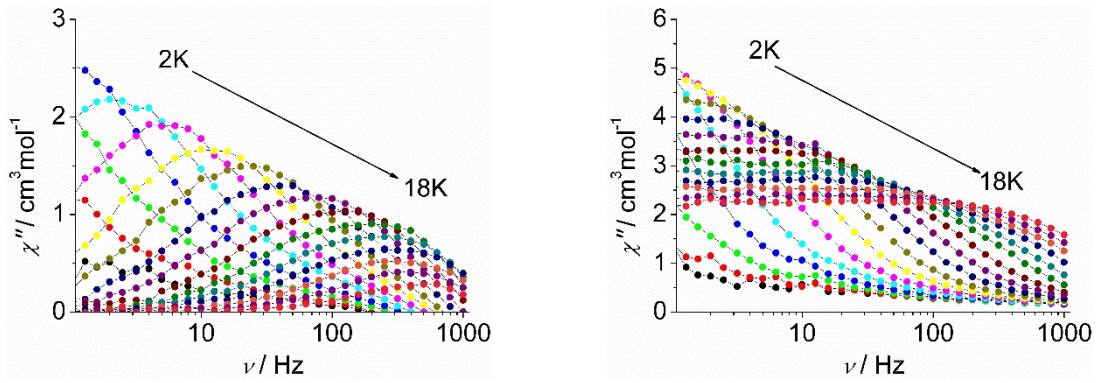

Fig. S18. Frequency dependence of the out-of-phase (χ'') and in-phase (χ') for **2a** under 1500 Oe dc field.

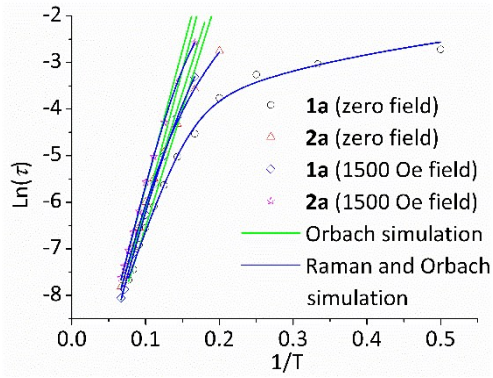

Fig. S19. Plot of ln(τ) vs 1/T for **1a** and **2a**. The green lines represent pure Arrhenius fitting at the high-temperature linear region under zero field and dc field. Blue lines correspond to the fitted results combining Orbach and Raman relaxation processes.

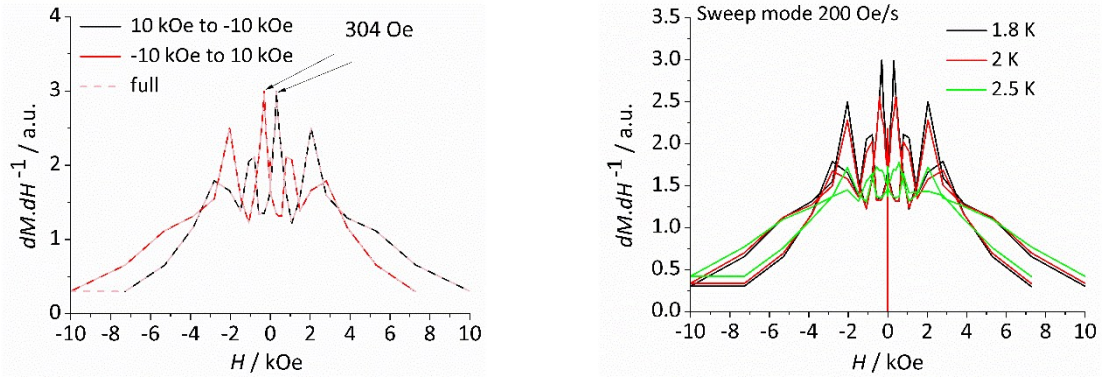

Fig. S20. The first derivative of magnetization (*dM*/*dH*) of complex **1Dy** versus magnetic field for the curves measured at 1.8 K (left) and different temperature (right) at scan rate of 200 Oe/s, sweep mode.

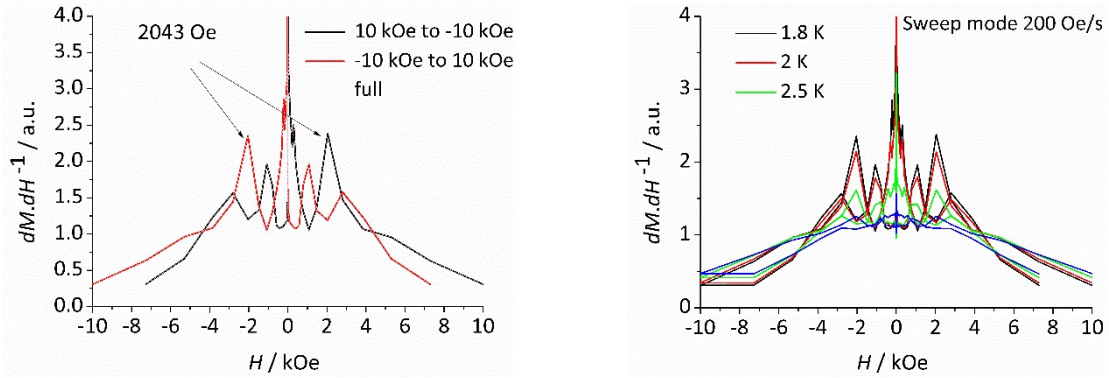

Fig. S21. The first derivative of magnetization (*dM*/*dH*) of complex **2Dy** versus magnetic field for the curves measured at 1.8 K (left) and different temperature (right) at scan rate of 200 Oe/s, sweep mode.